

# Multiple sea-ice states and abrupt MOC transitions in a general circulation ocean model

Yosef Ashkenazy · Martin Losch · Hezi Gildor ·  
Dror Mirzayof · Eli Tziperman

Received: 20 January 2012 / Accepted: 25 September 2012  
© Springer-Verlag Berlin Heidelberg 2012

**Abstract** Sea ice has been suggested, based on simple models, to play an important role in past glacial–interglacial oscillations via the so-called “sea-ice switch” mechanism. An important requirement for this mechanism is that multiple sea-ice extents exist under the same land ice configuration. This hypothesis of multiple sea-ice extents is tested with a state-of-the-art ocean general circulation model coupled to an atmospheric energy–moisture–balance model. The model includes a dynamic–thermodynamic sea-ice module, has a realistic ocean configuration and bathymetry, and is forced by annual mean forcing. Several runs with two different land ice distributions represent present-day and cold-climate conditions. In each case the ocean model is initiated with both ice-free and fully ice-covered states. We find that the present-day runs converge approximately to the same sea-ice state for the northern hemisphere while for the southern hemisphere a difference in sea-ice extent of about three degrees in latitude between the different runs is observed. The cold climate runs lead to

meridional sea-ice extents that are different by up to four degrees in latitude in both hemispheres. While approaching the final states, the model exhibits abrupt transitions from extended sea-ice states and weak meridional overturning circulation, to less extended sea ice and stronger meridional overturning circulation, and vice versa. These transitions are linked to temperature changes in the North Atlantic high-latitude deep water. Such abrupt changes may be associated with Dansgaard–Oeschger events, as proposed by previous studies. Although multiple sea ice states have been observed, the difference between these states is not large enough to provide a strong support for the sea-ice-switch mechanism.

**Keywords** Sea ice · Glacial-interglacial oscillations · Multiple sea-ice states · Oceanic general circulation model · MITgcm · Energy moisture balance model · Hysteresis

## 1 Introduction

Over the last million years (the late Pleistocene), Earth’s climate has experienced dramatic glacial-interglacial oscillations (Imbrie et al. 1984; EPICA-Community-Members 2004) with well established characteristics. The ice-sheets grow slowly (during  $\sim 90$  kyr) and melt much more rapidly (during  $\sim 10$  kyr). The Northern Hemisphere (NH) maximum ice-volume during the last glacial maximum (LGM) was about 15 times larger than today’s (Mix et al. 2001), with 2–3 km thick ice covering Canada and the Northern U.S. (Peltier 1994), and sea level that was lower by  $\sim 120$  m. The global temperature during the LGM was about 6 °C lower compared to present day and glacial atmospheric CO<sub>2</sub> concentration was lower by 80–100 ppm compared to interglacial times (Petit et al.

---

Y. Ashkenazy (✉) · D. Mirzayof  
Department of Solar Energy and Environmental Physics, BIDR,  
Ben-Gurion University, 84990 Midreshet Ben-Gurion, Israel  
e-mail: ashkena@bgu.ac.il

M. Losch  
Alfred-Wegener-Institut für Polar- und Meeresforschung,  
Bremerhaven, Germany

H. Gildor  
The Fredy and Nadine Herrmann Institute of Earth Sciences,  
The Hebrew University of Jerusalem, 91904 Jerusalem, Israel

E. Tziperman  
Department of Earth and Planetary Sciences and School  
of Engineering and Applied Sciences, Harvard University,  
Cambridge, MA, USA

1999). LGM winds were much stronger (Ram and Koenig 1997) compared with today's winds. The mechanisms underlying these massive changes are still not understood (e.g., Ghil 1994; Wunsch 2003).

Gildor and Tziperman (2000) suggested a “sea-ice switch” (SIS) mechanism for glacial-interglacial oscillations. According to this mechanism, sea-ice switches the climate system between a phase of growing ice sheets when the sea-ice extent is small (sea-ice switch is “off”), and a phase of retreating ice sheets when the sea ice extent is large (“on”). When the climate system is in its interglacial state and the sea-ice switch is “off”, the hydrological cycle is strong, and due to the resulting large snow accumulation rate, land ice gradually grows and its albedo cools the climate system. Eventually, after some 90 kyr, the high- and mid-latitude ocean reaches freezing temperature, leading to rapid sea-ice formation (sea-ice switch is “on”), resulting in strong atmospheric cooling and reduced evaporation from the ocean (because a significant fraction of the ocean is covered by sea ice and because of the reduced atmospheric temperature). The hydrological cycle and snow accumulation thus weaken while ablation (melting, ice streams, and calving) continues, and therefore land-ice sheets begin to retreat. With reduced ice sheets, the overall albedo is smaller and therefore the climate warms, sea ice melts (switching to “off”) again, and a new glacial cycle starts. For a more detailed description of the sea-ice switch mechanism see Gildor and Tziperman (2000, 2001) and Gildor (2003). The SIS mechanism and its associated rapid sea-ice changes have been used to explain glacial cycles, Dansgaard–Oeschger (DO) oscillations and Heinrich events, using various simple models (Gildor and Tziperman 2000; Tziperman and Gildor 2003; Timmermann et al. 2003; Ashkenazy and Tziperman 2004; Sayag et al. 2004; Kaspi et al. 2004; Tziperman et al. 2006; Wang and Mysak 2006; Loving and Vallis 2005). The important implication for the present study is that the SIS mechanism implies multiple equilibria of sea ice for a given continental ice volume, and a sea-ice hysteresis as continental ice varies (Fig. 1). The numerical experiments described below aim at capturing the multiple states of the sea ice when starting from two extreme initial conditions (i.e., ice-free and ice-covered ocean) under the same land-ice coverage; we do not attempt to reproduce the entire hysteresis loop of the SIS mechanism. The existence of multiple states of sea ice under the same land-ice configuration in a state of the art ocean model would provide support for the SIS mechanism.

Several studies have shown multiple sea-ice states using various models. Specifically, Langen and Alexeev (2004) used the community atmospheric model (CAM) (Holland et al. 2006a) coupled to a simple slab ocean model under aqua-planet and annual mean conditions, and demonstrated

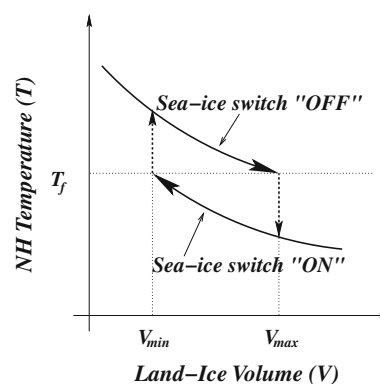


**Fig. 1** Schematic of the hysteresis loop and the multiple sea ice and temperature states under the same continental ice volume. The arrows indicate the direction of the hysteresis loop.  $T_f$  indicates the freezing temperature of sea water,  $V_{min}$  the minimum land-ice volume, and  $V_{max}$  the maximum land-ice volume. Starting from the upper branch of the hysteresis loop (SIS is “off”), land ice becomes more extensive and temperature drops as a result of the ice-albedo feedback. Once reaching the freezing temperature of sea water, an extensive sea ice is formed (SIS is “on”) which result in significantly reduced net precipitation and thus shrinking land ice sheets. This will lead to an increase in temperature until temperature will raise above the freezing temperature at which the sea ice will melt, causing the SIS cycle to start again. See text form more details

the existence of multiple states of sea-ice extent under the same parameters. The control parameter in their experiments was the oceanic “qflux” (i.e., prescribed flux representing ocean heat transport); three sea-ice extents were identified: (1) ice-free ocean, (2) intermediate sea-ice extent up to the high latitudes, and (3) extensive sea-ice extent (up to the mid-latitudes). Ferreira et al. (2011) used a coupled ocean-atmosphere version of the MITgcm (MITgcm Group 2010), but without sea-ice dynamics, in an aqua planet configuration and again identified three different states of sea ice: polar ice-cap extending to the mid-latitudes, ice free and snowball states. We take a complementary approach of using a full ocean general circulation model (GCM) with a dynamics-thermodynamic sea-ice component, coupled to a simple atmospheric model, and use realistic continental geometry and ocean bathymetry. Our simpler and computationally efficient GCM gives us larger flexibility in exploring the parameter space. In a different study, Marotzke and Botzet (2007) varied the solar constant in a coupled atmosphere–ocean GCM and showed that once the climate is sufficiently cold to enter a snowball state, a much larger radiation constant is needed to “escape” from such a state; this study thus showed multiple sea-ice states under the same solar radiation input. Recently, Abbot et al. (2011) suggested that multiple states of sea ice can arise due to the difference in albedo between dark, bare sea ice and bright, snow covered sea ice. Eisenman et al. (submitted) have used a fully coupled atmosphere-ocean GCM to study the DO events and

demonstrated the possibility of two quasi-stable sea-ice states, associated with the stadial and interstadial phases of the DO events; the interstadial state converged to the stadial state after  $\sim 700$  hundreds years of simulations. Recent studies (Eisenman and Wettlaufer 2009; Lindsay and Zhang 2005; Overpeck et al. 2005; Serreze and Francis 2006; Holland et al. 2006b; Maslanik et al. 2007; Lenton et al. 2008; Merryfield et al. 2008) discussed the possibility of a tipping point in the Arctic sea ice cover (below which the Arctic will be ice free) and associated this point with hysteresis and multiple equilibria. However even more recent studies suggested that there is no tipping point in the Arctic sea-ice (e.g., Tietsche et al. 2011).

The main goal of this study is to test whether multiple states of sea ice exist under the same land ice cover in a realistic-geometry state-of-the-art ocean-ice model coupled to a simple atmospheric model. This goal is explored for both “*present day*” and for “*cold*” climates. We show that such multiple sea-ice states indeed exist in the model, although they are not as pronounced in the NH as predicted by the sea-ice switch mechanism. We note that the model

used here, while using realistic geometry, still lacks many feedbacks and processes. We also examine rapid sea-ice changes in these model runs and consider their relevance to observed rapid climate change.

The paper is organized as follows: the model is described in Sect. 2, the experiments performed with the model are described in Sect. 3, followed by analysis of the meridional overturning circulation (MOC) and the sea-ice extent (Sect. 4); discussion and conclusions are presented in Sect. 5.

## 2 Model description and spinup

### 2.1 The oceanic model—MITgcm

The Massachusetts Institute of Technology ocean general circulation model (MITgcm) solves the primitive equations (Marshall et al. 1997a, b) and is used here in a global cubed-sphere configuration (Adcroft et al. 2004) with a lateral resolution of about 290 km (varying from 330 km

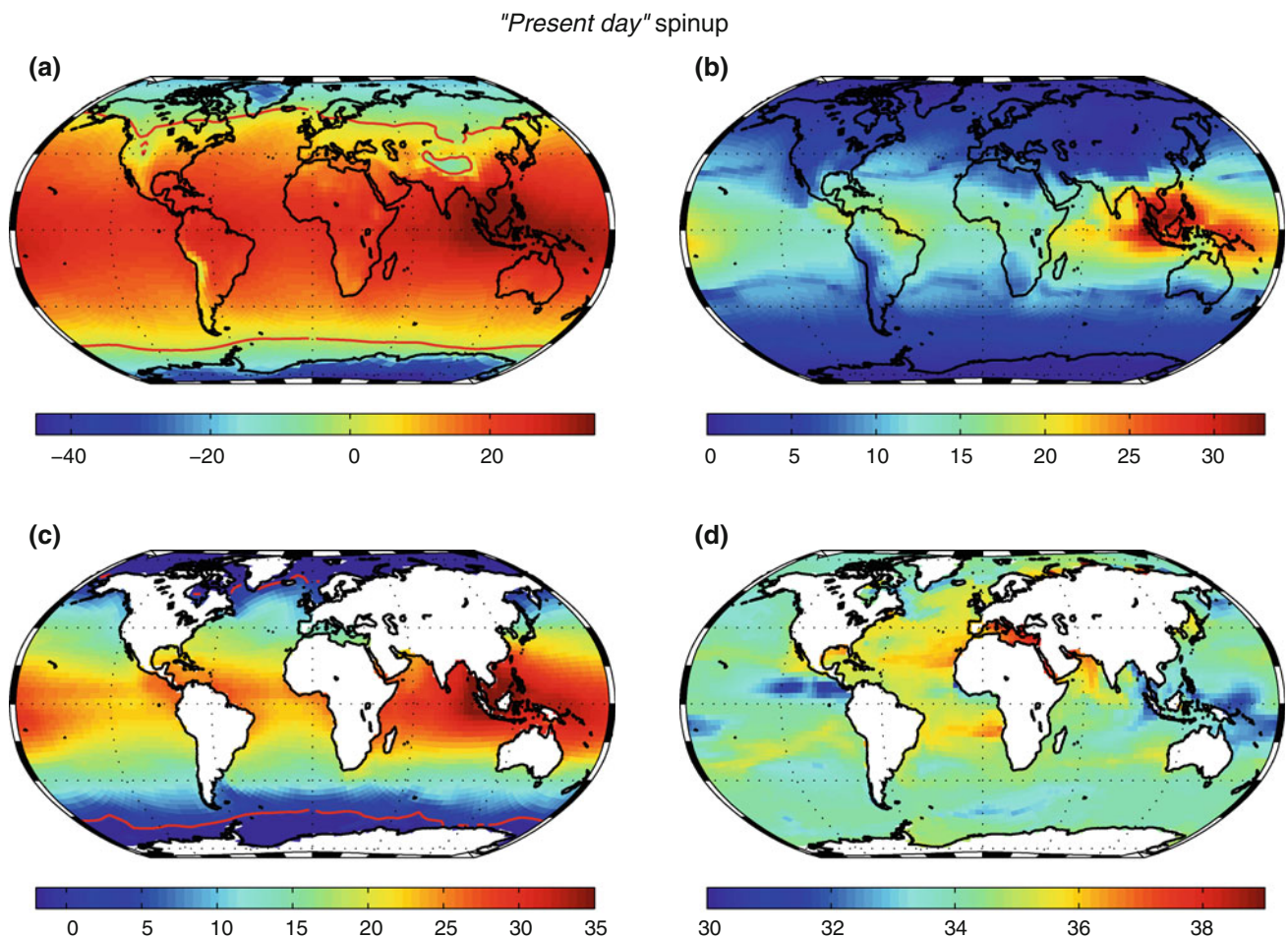


**Fig. 2** Maps at the end of the “present day” 4,000 years spinup run, of **a** air temperature ( $^{\circ}\text{C}$ ), **b** air humidity ( $\text{g/kg}$ ), **c** sea surface temperature (SST,  $^{\circ}\text{C}$ ) and **d** sea surface salinity (SSS, ppt). The red contour line is  $0^{\circ}\text{C}$  temperature iseline

resolution at the center of a cube-sphere face to 110 km at face corners). The ocean has 15 vertical levels, with thicknesses ranging from 50 m for the surface layer to 690 m for the bottom layer. We use the isopycnal eddy parametrization scheme of Gent and McWilliams (1990) and Redi (1982). The vertical background diffusion coefficient for both temperature and salinity is  $3 \times 10^{-5} \text{ m}^2/\text{s}$ , and the vertical viscosity is  $10^{-3} \text{ m}^2/\text{s}$ . In addition, the k-profile parameterization (KPP, Large et al. 1994) scheme is used to simulate vertical mixing and deep convection processes.

## 2.2 The dynamic-thermodynamic sea-ice model

The sea-ice component of the MITgcm is used to simulate sea ice with a viscous-plastic rheology. Ice velocities advect effective ice thickness (volume), ice concentration and snow with a flux-limiting scheme. Ice formation and melting with zero-layer thermodynamics follows Semtner (1976) and Hibler (1980). The ice model exchanges heat and fresh water with the ocean and the atmosphere at each

ocean time step. The load of the ice and snow depresses the sea-surface of the ocean to account for exact mass-balance (Campin et al. 2008). Further details of the model are described in Losch et al. (2010) and references therein.

## 2.3 The atmospheric energy–moisture-balance model

The atmospheric model is based on the energy moisture balance model (EMBM) of Fanning and Weaver (1996) and the atmospheric component of the UVic Earth System Climate Model (Weaver et al. 2001) as follows. Our EMBM consists of one vertical layer and a horizontal grid that coincides with the oceanic grid. Two prognostic variables, atmospheric temperature,  $T_{\text{air}}$ , and humidity,  $q_{\text{air}}$ , are updated with a second order Adams–Bashforth scheme. Surface winds are prescribed and humidity is advected by these winds. Topographic effects on temperature and humidity are taken into account by assuming a prescribed lapse rate of 6 K/km. Atmospheric  $\text{CO}_2$  concentration is also taken into account.

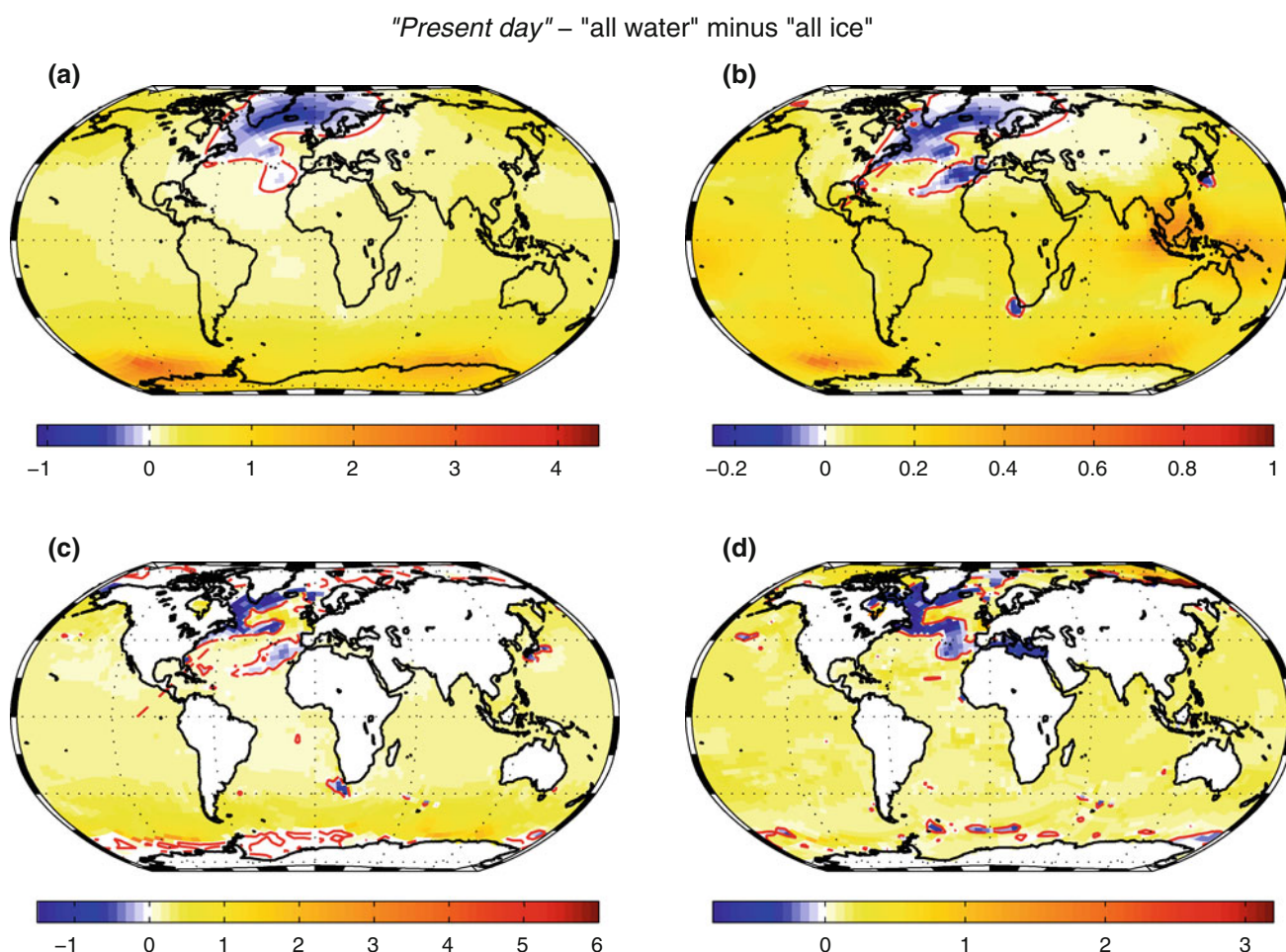


**Fig. 3** The difference between the "all water" and "all ice" runs of the "present day" experiments. **a** Air temperature (°C), **b** air humidity (g/kg), **c** SST (°C), and **d** SSS (ppt) are shown. The red contour line indicates the zero value

The main difference from Weaver et al. (2001) is the treatment of surface albedo to include the effect of land ice albedo on short wave reflection. Over the ocean the albedo is set to a constant (0.07) while the sea-ice model computes the albedo over sea ice as a function of snow cover and temperature. Land surface is assumed to have no heat capacity, but spatially varying land albedos can be prescribed. The land albedo is set to that of land ice (0.6) over prescribed land ice cover. Shortwave radiation is scattered once while passing through the atmosphere, and is then reflected at the surface according to the albedo and scattered a second time on its way up through the atmosphere into space.

The atmospheric time step is set to 10 min, so that the atmosphere is stepped multiple times within a single ocean tracer time step of one day. The tracer acceleration method of (Bryan 1984) is used for efficiency, with a momentum time step of 20 min. This approach is not expected to lead to major biases in steady solutions with the time-independent forcing used here. The atmospheric model exchanges

heat and fresh water with the surface at each ocean model time step. At the beginning of the ocean time step, the atmosphere computes heat and fresh water fluxes based on the ocean and ice state of the previous time step and averages them over the ocean time step while stepping the atmospheric variables forward in time. Then the sea ice and ocean models are stepped forward.

## 2.4 Spinup

The ocean model was initiated with present-day salinity and temperature fields (Levitus 1982), and the coupled ocean-sea ice-atmosphere model was then run for 4,000 years to reach a quasi steady state. The air temperature, air humidity, sea-surface temperature (SST) and sea-surface salinity (SSS) at the end of the “*present day*” spinup run are presented in Fig. 2. Overall, the model has all relevant features to be expected from a coarse model with an EMBM atmosphere (Weaver et al. 2001), although

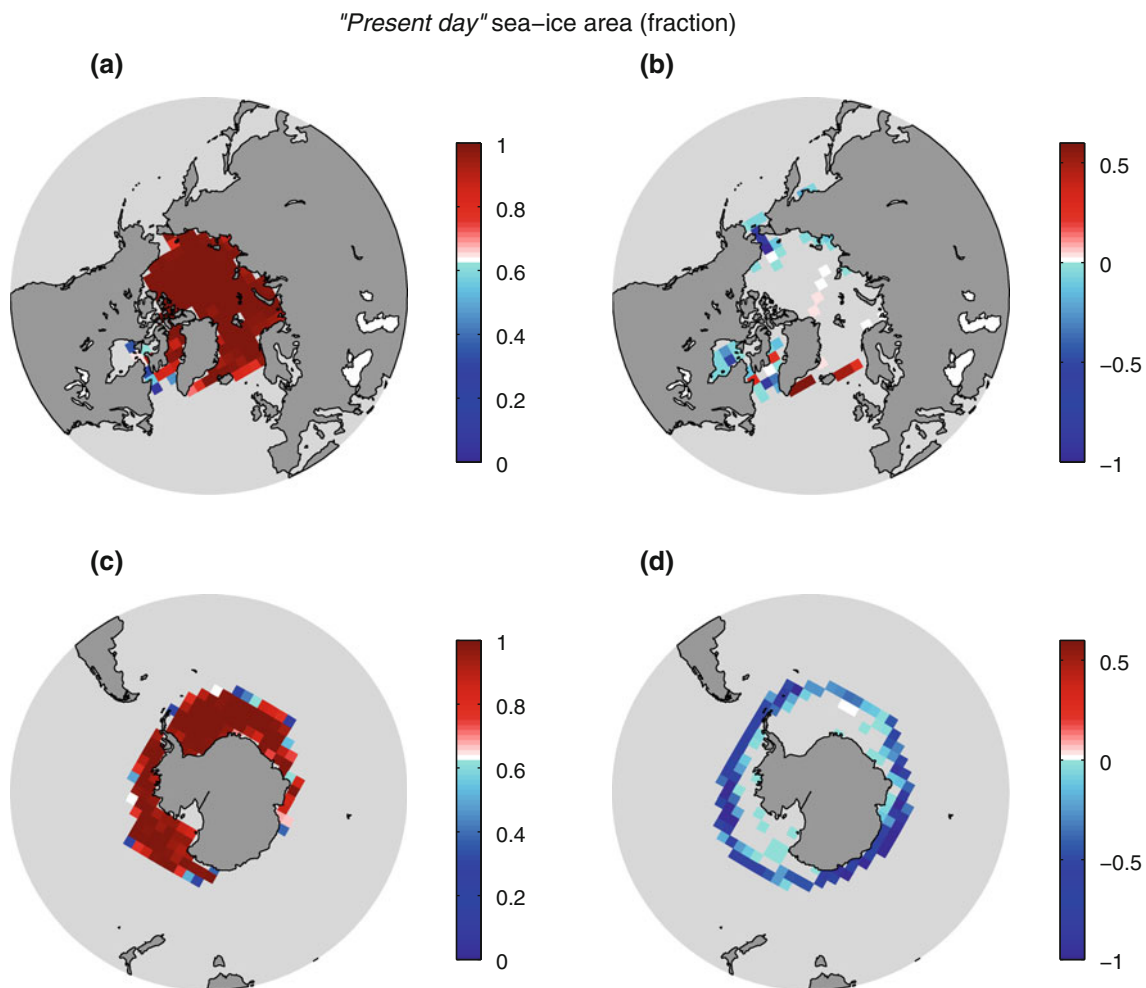


**Fig. 4** a NH and c SH sea-ice area (in fraction) for the “*present day*” “all water” experiment. b, d Depict the difference between the “all water” and the “all ice” runs

atmospheric humidity and sea-surface salinity exhibit large deviations from observation. This is most probably due to the simplistic form of precipitation of the model, as was also indicated by Fanning and Weaver (1996).

In addition to the “*present-day*” spinup run we performed similar spinup runs for the “*cold-climate*” setups described in Sect. 2.5. To achieve the cold conditions required for some of our numerical experiments we prescribed land-ice albedo over land at latitudes 40–90°N, sea-ice albedo of 1, and atmospheric CO<sub>2</sub> level of 180 ppm. These values are not meant to be realistic, but are used to explore an extreme regime of parameter space.

## 2.5 The numerical experiment

Three initial states are used, hereafter referred to as “*present day*”, “*cold climate 1*”, and “*cold climate 2*”. For each of these, two runs were performed, one with an initially ice-free ocean (“*all water*” initial conditions) and one with an ocean that is initially fully covered by sea ice (“*all*

ice” initial conditions). The purpose of the runs is to explore the multiple states schematically suggested by Fig. 1. All runs were started from the final state of the spinup runs, except for sea ice, free surface, and upper ocean temperature. These fields were adjusted according to the different initial sea-ice conditions. The runs were integrated for 10,000 years; quasi-steady states were reached after ~2,000 years. We now consider the results of these 2,000 years of integration. The different runs are specified according to the initial conditions as follows.

1. “*Present day*” experiment: “*present day*” land ice and initial conditions of (1) no sea ice and (2) 10 m thick sea ice covering the entire ocean and a corresponding negative free surface anomaly to preserve the water content of the model (this is referred to below as the “*all ice*” initial state). Note that the model does not enter a snowball state in the last configuration, because of the relatively warm initial ocean temperatures.
2. “*Cold climate 1*” experiment: land ice albedo for latitudes 40–90°N, sea-ice albedo set to 1, atmospheric

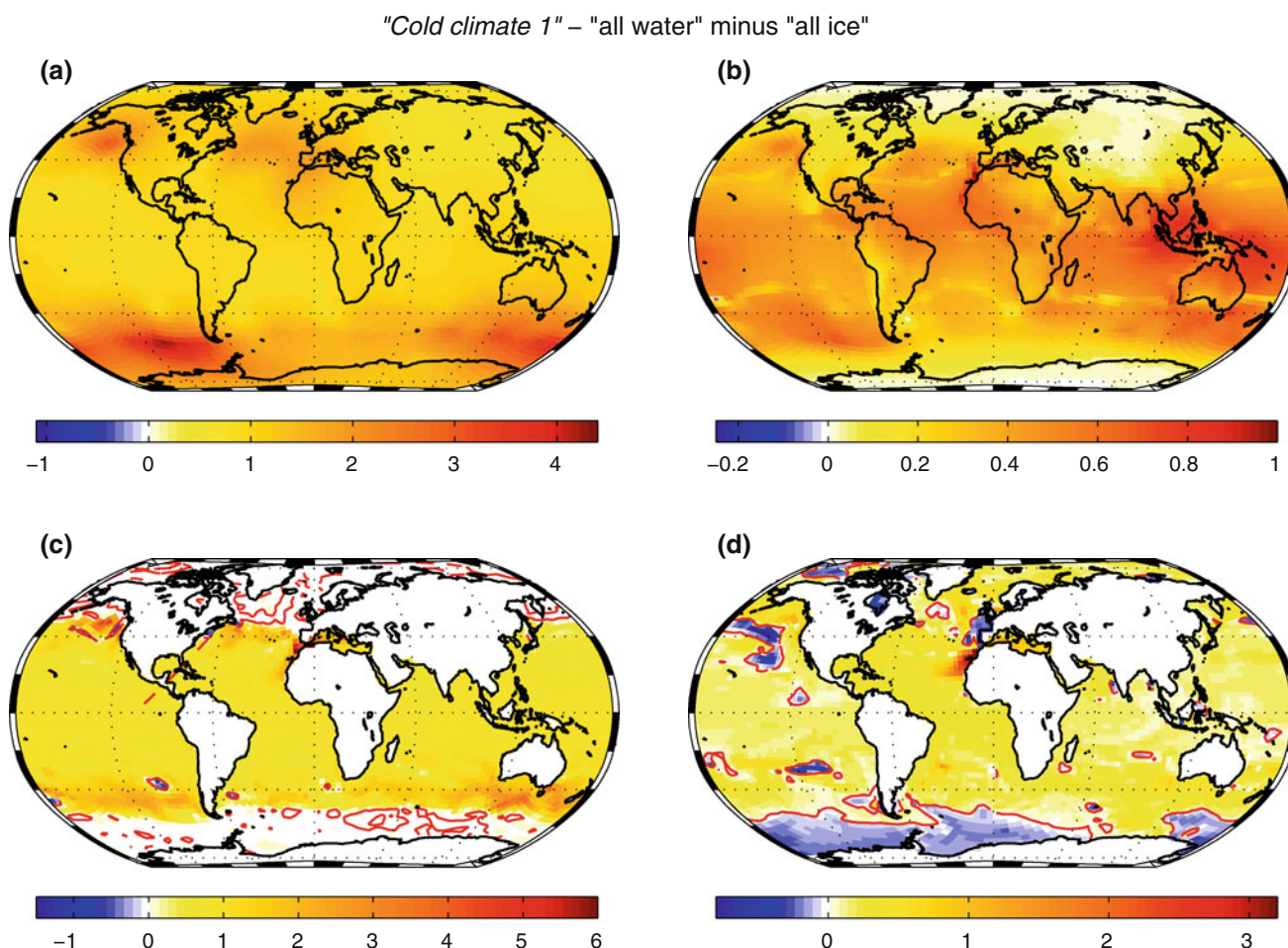


**Fig. 5** The difference between the “*all water*” and “*all ice*” runs of the “*cold climate 1*” experiments. **a** Air temperature (°C), **b** air humidity (g/kg), **c** SST (°C), and **d** SSS (ppt) are shown. The red contour line indicates the zero value

CO<sub>2</sub> level of 180 ppm, and increased atmospheric albedo profile specified as function of latitude. Two initial conditions were again considered, (1) ice free ocean and (2) “all ice” initial state, and upper layer ocean (to a depth of 50 meters) that is 10 °C lower than that of the spinup run (but not lower than the ocean freezing temperature). The prescribed upper ocean cooling is meant to ensure convergence to a cold state if it exists.

3. “Cold climate 2” experiment: Same as the “cold climate 1” experiment but with a higher-yet atmospheric albedo profile (increase of  $\sim 1\%$  compared to “cold climate 1”, equivalent to a decrease of  $\sim 2\text{ W/m}^2$  in the incoming short-wave radiation), to yield an even colder climate ( $\sim 1\text{ °C}$  difference in mean ocean temperature).

The purpose of starting with both an ice-free ocean (“all water”) and ocean that is completely covered by sea ice (“all ice”) is to find multiple sea-ice states if they do exist, i.e., converging to the multiple sea-ice states from above and below the curves presented in Fig. 1. The use of both “present day” and “cold climate” experiments should explore the sensitivity of the results to a wide range of climate conditions. In designing these experiments, many different initial conditions for temperature, ice and different atmospheric CO<sub>2</sub> concentration scenarios were tested. Here we present only those experiments that most clearly demonstrate the existence of multiple sea-ice states. The steady states presented in Fig. 2 were used to initiate the model with either the “all water” or “all ice” initial states discussed in previous section; we performed a similar spinup run for the “cold climate” experiments.

### 3 Multiple sea-ice equilibria

#### 3.1 “Present day” experiment

Consider first the runs starting from the “present day” steady state. After a 2,000 year simulation, the “all water” run lead to fields that are very similar to the steady-state fields shown in Fig. 2. The difference between the “all water” and “all ice” runs are shown in Fig. 3. We show below (Sect. 3.4) that the runs converged close to a steady state within this period. For air and sea surface temperature, the “all ice” run exhibits colder temperatures (up to 2.5 °C difference) over some parts of the Southern Ocean where there is a difference in sea-ice cover, as shown below.

Higher humidity in the “all water” run is associated with higher atmospheric temperatures, following the Clausius–Clapeyron relation. Some regions, such as the western tropical Pacific, show higher humidity values for the “all water” run accompanied by a relatively small

temperature difference in that region. This strong humidity response to a small temperature difference is due to the exponential dependence of moisture on temperature. The SSS differences between the “all water” and “all ice” runs may be mainly attributed to melting and formation of sea ice, as these occur in the high latitudes of both hemispheres.

The “present day” runs’ sea-ice area at the end of the 2,000 years of simulations are depicted in Fig. 4. The difference between the sea-ice area of the “all water” run and the “all ice” run is small and not spatially coherent in the NH, while it is larger and coherent in the Southern Hemisphere (SH) (approximately 3° latitude). The change in sea-ice cover is consistent with the other fields depicted in Fig. 3. We conclude that “present day” land ice conditions do not lead to multiple sea-ice states with the modeling setup used here in the NH. There are two distinct sea ice states in the SH, yet the differences between these two states are small.

#### 3.2 “Cold climate 1” experiment

The difference between the “all water” and “all ice” runs of the “cold climate 1” experiment is shown in Fig. 5. Unlike the “present day” runs shown in Figs. 2, 3 and 4, it is clear that the “all water” run has a globally warmer atmosphere compared to the “all ice” run. In addition, the difference between the results using the “all water” and “all ice” initial conditions is larger than for the “present day” experiment, with maximum differences of more than 4 °C for air temperature and more than 5 °C for SST. The largest temperature difference is over the Southern Ocean and the North Pacific, consistent with the differences in sea-ice cover shown in Fig. 6. Consistent with the air temperature, the “all water” run atmosphere is globally more humid, with higher values over the west-Pacific warm pool, as expected from the relatively high SST over this region. As in the “present day” experiment, the “cold climate 1” experiment exhibits a higher humidity response to a small temperature difference between its two runs over warm regions such as the western Pacific. The SSS difference between the “all water” and “all ice” runs has relatively large amplitudes in regions that experienced changes in sea-ice cover; on average the “all ice” surface water appears saltier, most likely because greater sea ice production causes more brine rejection that in turn increases the surface salinity.

The sea-ice area maps of the two “cold climate 1” runs are presented in Fig. 6. The sea-ice extends further equatorward compared to the “present day” runs (Fig. 4); it reaches the northern part of Mediterranean Sea, covers extensive parts of the North Pacific, and reaches South America in the Southern Ocean. In addition, the “all ice”

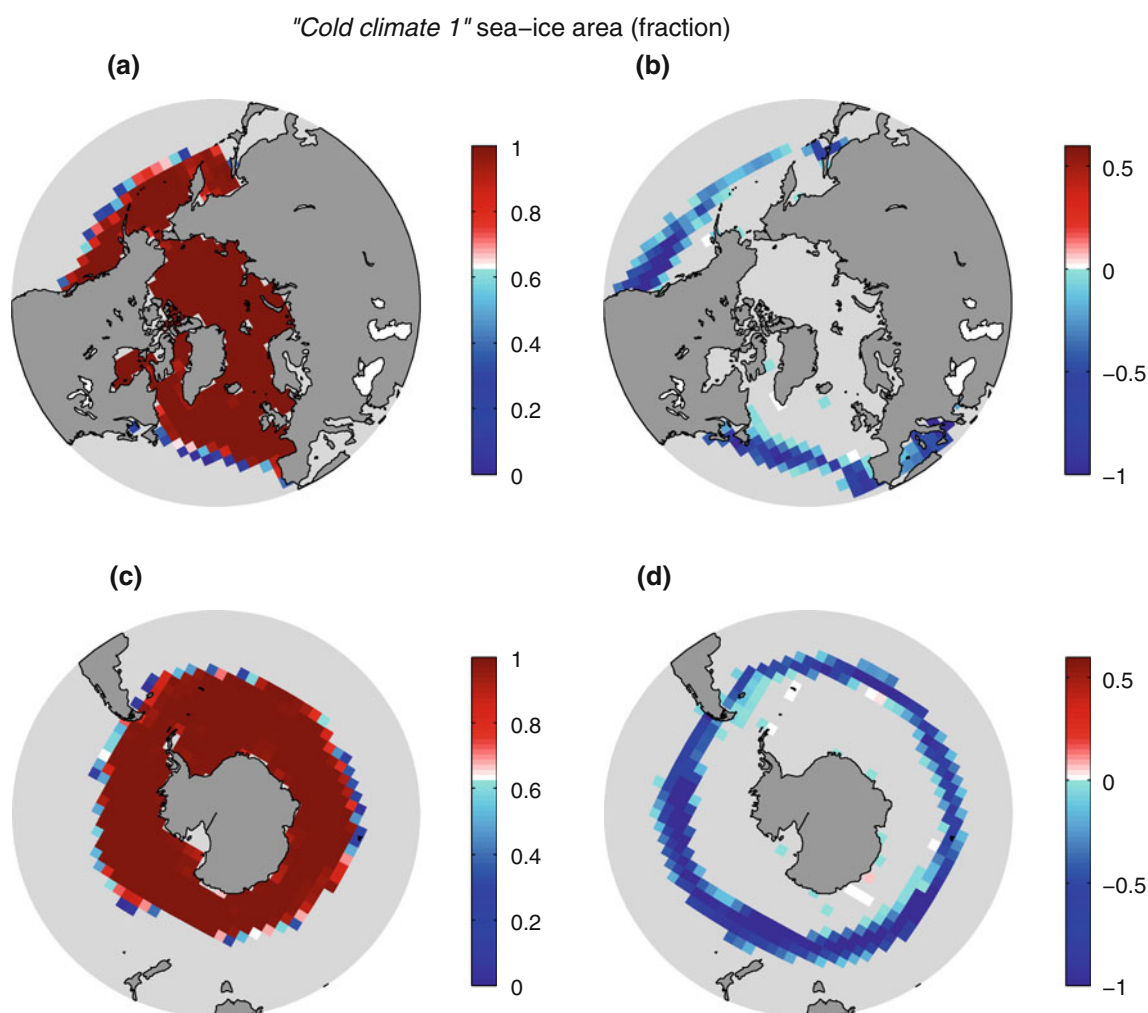


**Fig. 6** **a** NH and **c** SH sea-ice area (in fraction) for the “cold climate 1” “all water” experiment. **b**, **d** Depict the difference between the “all water” and the “all ice” runs

sea-ice clearly exceeds that of the “all water” run by  $4^\circ$  in latitude. The “cold climate 1” basic state thus supports multiple states of sea ice.

### 3.3 “Cold climate 2” experiment

In the “cold climate 2” experiment we increased the atmospheric albedo even more (by 0.018 at the equator and 0.002 at the high latitudes), resulting in an even colder climate with a larger sea-ice extent. The “all ice” sea-ice extent exceeds that of the “all water” run by  $4^\circ$  in latitude, similar to the “cold climate 1” experiment (Fig. 7e, f, h, i).

### 3.4 Comparison between the experiments

The evolution of the North Atlantic (NA) maximum meridional overturning circulation (MOC), the NH and NA sea-ice extent, and the SH sea-ice extent are presented in Fig. 7. The extent of the sea ice is calculated as the latitude

at which the zonal-mean sea-ice area fraction drops below 0.5. For the “present day” experiment there is a quick convergence to a single state of the MOC and NH sea ice while there are two distinct sea-ice states in the SH, with sea-ice extents that differ by about  $3^\circ$  in latitude.

The “cold climate 1” and “2” experiments both remain in very different quasi-equilibrium for some time, but then change into their steady states, yet in different ways. In both runs, the quasi-equilibrium states have distinct MOC amplitudes and corresponding different NH sea-ice states. The “all water” run is initially associated with the stronger MOC state and the “all ice” with the weaker MOC state. In the “cold climate 1” runs the weak MOC state jumps to the stronger MOC state after about 1,500 years of simulations, and simultaneously the NH sea ice edge moves northward toward the “all water” sea-ice extent. We did not observe significant further changes for the remaining 8,000 years of the simulations (not shown). In an opposite transition in the “cold climate 2” run, the stronger NA MOC state collapses

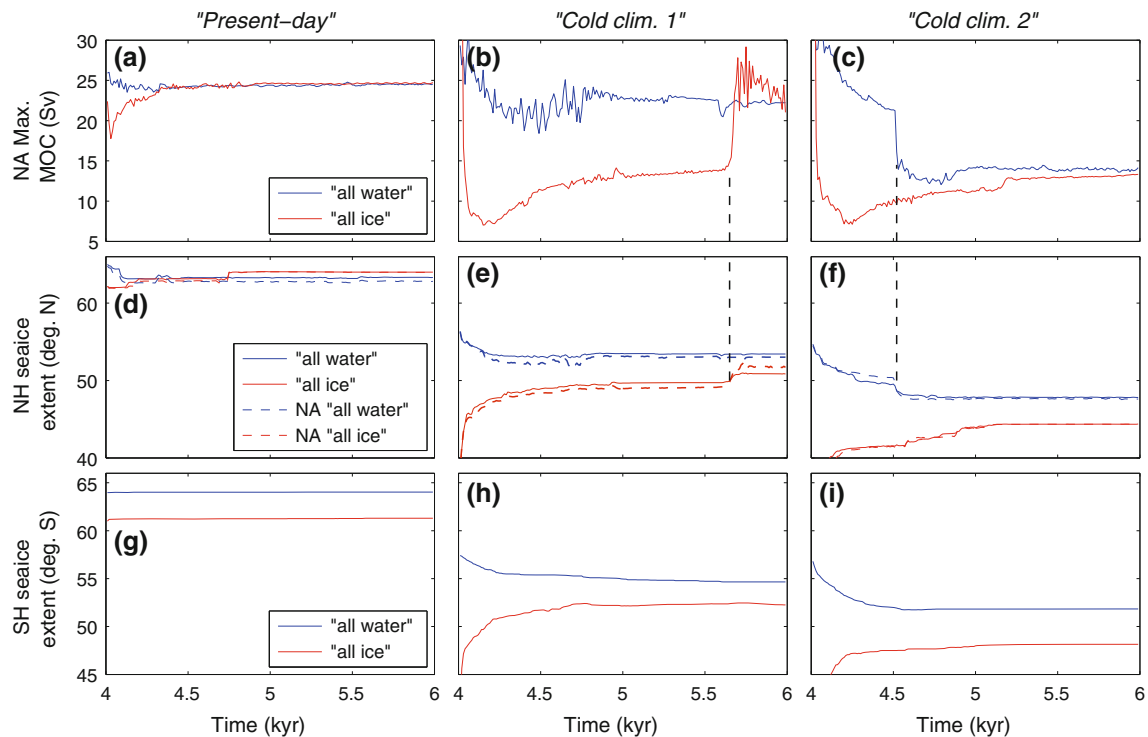


**Fig. 7** Time evolution of maximum NA meridional overturning circulation (MOC, **a**, **b**, **c**), NH sea-ice extent in degree N (**d**, **e**, **f**), and SH sea-ice extent in degree S (**g**, **h**, **i**) for the “present day” (**a**, **d**, **g**), “cold climate 1” (**b**, **e**, **h**) and “cold climate 2” experiments (**c**, **f**, **i**). Both “all water” (blue) and “all ice” (red) are included where for the

NH sea-ice extent the NA values are also included (dashed-blue for the “all water” run and dashed-red for the “all ice” run). The vertical dashed lines indicate the time of transition from one MOC state to another

to the weaker state after about 500 years of simulation; the NH sea-ice edge in the “all water” run simultaneously moves further southward. These abrupt transitions are further discussed in the next section. The model seems to support fairly long-lasting and significantly different multiple quasi-equilibria, and one wonders if some change in the model formulation could stabilize these quasi-equilibria so that they can last indefinitely.

The Southern-Ocean sea ice does not exhibit any abrupt transitions. The difference between the Southern Ocean sea-ice extent of the “all ice” run and the “all water” run in the three different experiments (“present-day” and “cold climate 1 and 2”) varies between three and five degrees latitude (Fig. 7), where a larger difference is observed in the coldest experiment (“cold climate 2”).

#### 4 Meridional overturning circulation stability and NH sea-ice extent

The interaction of the MOC and sea-ice extent has been discussed in many previous studies (e.g., Manabe and Stouffer 1999; Kaspi et al. 2004; Timmermann et al. 2003; Gildor and Tziperman 2003; Wang and Mysak 2006; Loving and Vallis 2005; Colin de Verdière and Te Raa 2010; Arzel

et al. 2010, 2011). Freshening of the high-latitude NA creates a layer of light water that results in reduced formation of deep water and hence leads to an MOC shutdown and increased sea ice extent. When the MOC is restarted (Winton 1993), warm low latitude water reaches the high latitudes and thus reduces the sea ice extent.

We find that the transitions between the different MOC states are linked to changes in deep ocean temperatures, following the relaxation oscillation mechanism of Winton (1993) (see also Winton and Sarachik 1993; Ashkenazy and Tziperman 2007). In this mechanism deep ocean heat diffusion (i.e., parameterized eddy flux) from the low latitudes results in a warming of the deep high-latitude ocean (while the same eddies do not affect the surface ocean because it is strongly coupled to the atmosphere). This weakens vertical stratification in the high latitudes and eventually leads to restarted convection and an abrupt MOC increase.

Figure 8 shows the zonal mean NA water temperatures as a function of depth and time for the “cold climate 1” “all ice” and “cold climate 2” “all water” runs, averaged over both 50–70°N and 70–90°N. The latitude range 50–70°N is closely associated with changes of the sea ice and the MOC. For the “cold climate 1” “all ice” run, the 50–70°N deep water becomes warmer with time, and the

stratification becomes weaker, until it is sufficiently weak to allow deep convection and the MOC to abruptly restart (Fig. 7b). After the transition (occurred at  $t \approx 5.65$  kyr), the MOC slightly and gradually weakens between 5,700–6,000 years. The switch to a stronger NA MOC state results in a reduced NH sea-ice extent as shown in Fig. 7e. A different picture is seen at the higher latitudes, 70–90°N, where the deep ocean becomes significantly warmer after the transition to a stronger MOC. This is likely the outcome of the stronger MOC heat transport.

In the “cold climate 2” “all water” run, there is a switch from a stronger MOC state to a weaker state (Fig. 7c). Prior to this transition (at  $t \approx 4.52$  kyr), the 50–70°N stratification (Fig. 8c) becomes stronger with time as the deep water cools, until the MOC switches to its weaker state. This transition is accompanied by a equatorward extension of sea ice (Fig. 7f). After the transition the stratification weakens within the 50–70°N band and the deep ocean warms. At the high latitudes (70–90°N) the surface layer warms (and thus gains buoyancy), and subsequently the deep water warms.

Figure 9 shows the zonal mean NA salinity as a function of time. Note that the uppermost ocean is fresh when the

MOC is weak and vice versa, both for 50–70°N and 70–90°N. In addition, deep ocean at very high latitudes of the NA freshens with time when the MOC is weak, possibly because of diffusion of fresh water from the upper ocean. This freshening ceases when the MOC state changes or when a steady state is reached, and does not occur at 50–70°N. Interestingly, the deep water of the very high latitudes of the NA of the “Cold clim. 1” “all ice” experiment warms abruptly at 5 kyr (Fig. 8b). This rapid warming may be related to the increased mid-depth salinity of the “Cold clim. 1” “all ice” experiment (Fig. 9b) and corresponding changes to the stratification and vertical stability.

Figures 10, 11 and 12 show the NA MOC and the zonal mean temperature and salinity before and after the transitions, for the “cold climate 1” “all ice” and “cold climate 2” “all water” runs. The northern edge of the NA MOC cell approximately coincides with the extent of the sea ice, consistent with previous studies that often find deep water formation near the sea ice edge (e.g., Schmittner et al. 2003). Figure 11 shows that the surface water after the transition of the “cold climate 1” “all ice” run (at 35–55°N) is warmer while the deep water is colder

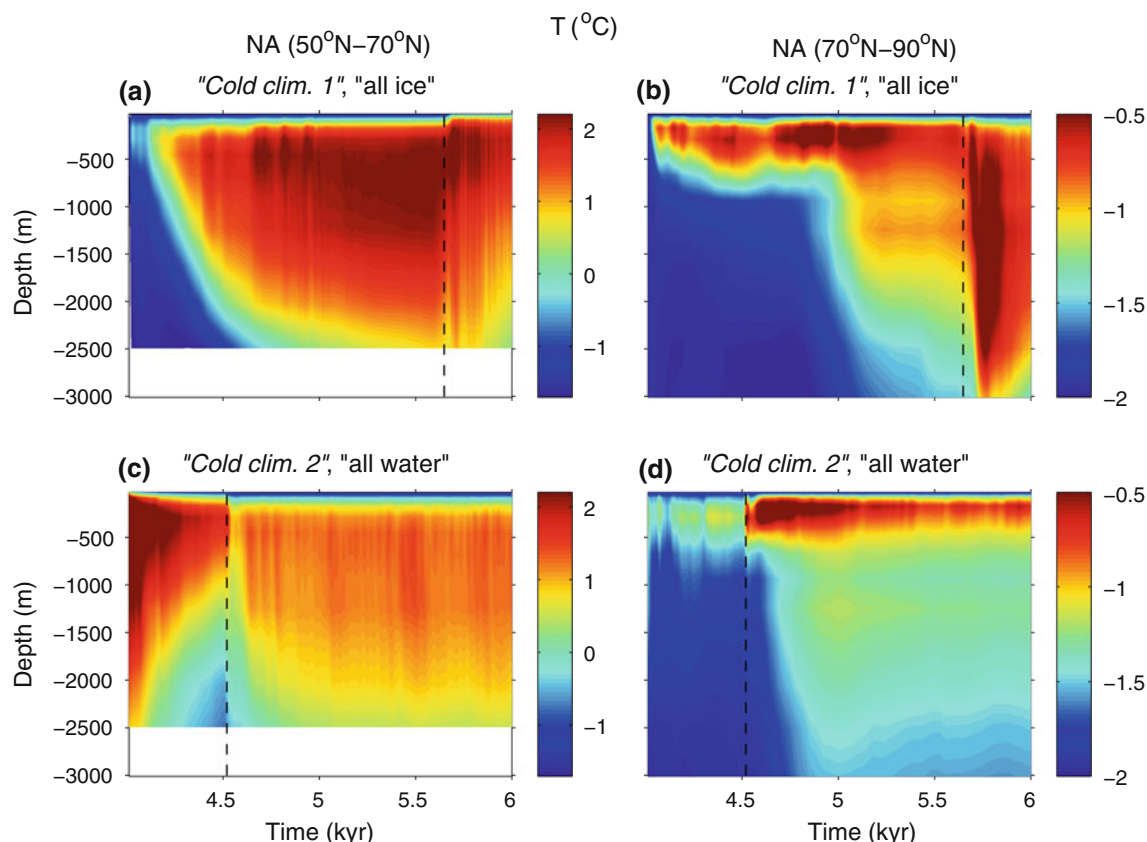


**Fig. 8** Time evolution of the NA zonal mean ocean temperature for different depths, for 50–70°N (a, c) and 70–90°N (b, d), for the “cold climate 1” (a, b) and “cold climate 2” (c, d) experiments. The vertical dashed lines indicate the time of transition from one MOC state to another

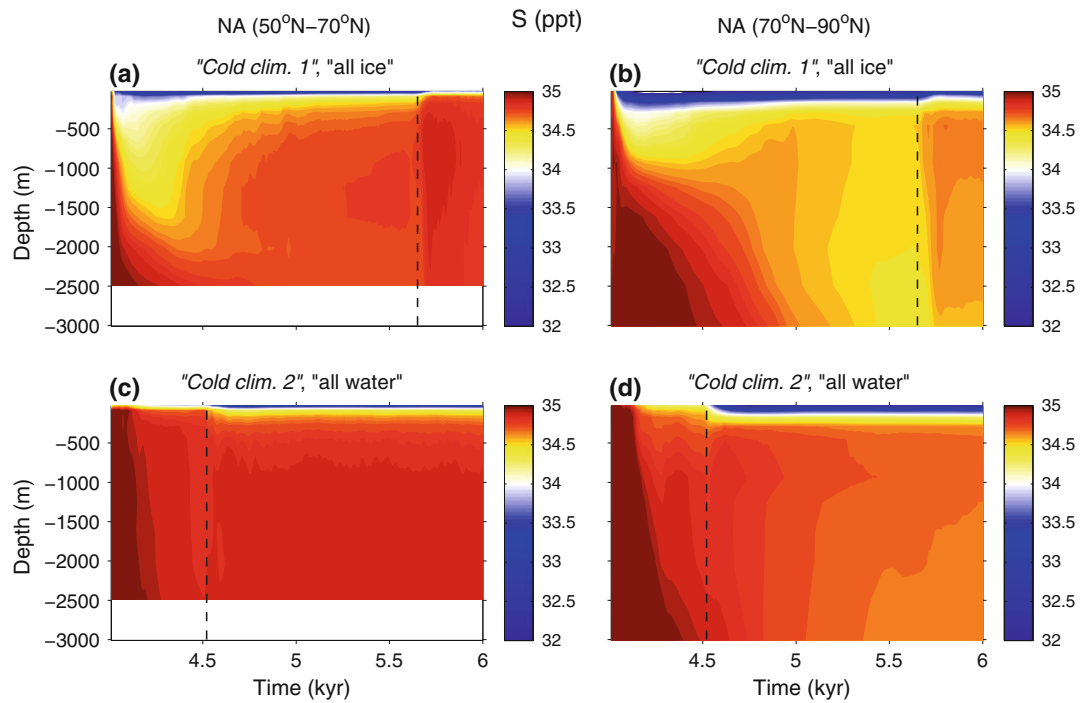


**Fig. 9** Time evolution of the NA zonal mean ocean salinity for different depths, for 50–70°N (a, c) and 70–90°N (b, d), for the “cold climate 1” (a, b) and “cold climate 2” (c, d) experiments. The vertical dashed lines indicate the time of transition from one MOC state to another

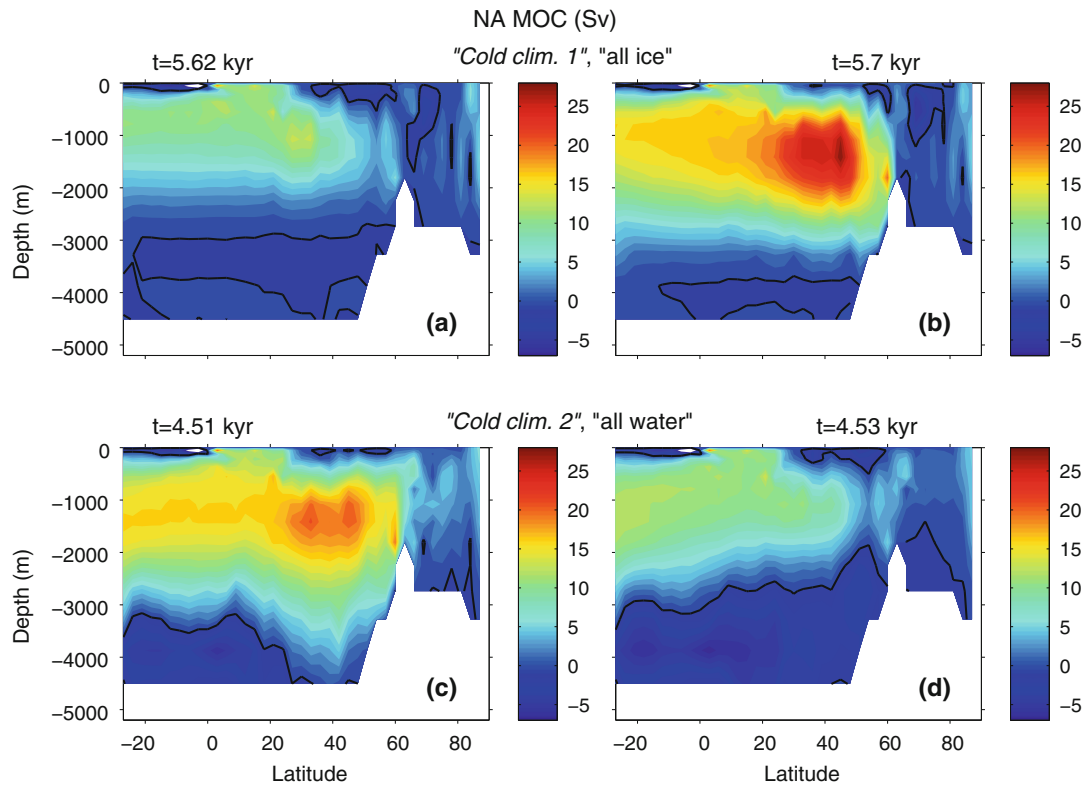


**Fig. 10** The NA meridional overturning circulation before (a, c) and after (b, d) the transitions indicated by the vertical dashed lines in Figs. 7 and 8, for the “cold climate 1” “all water” (a, b) and “cold

climate 2” “all ice” (c, d) runs. The black contour line indicates the zero value while positive value indicate clockwise circulation

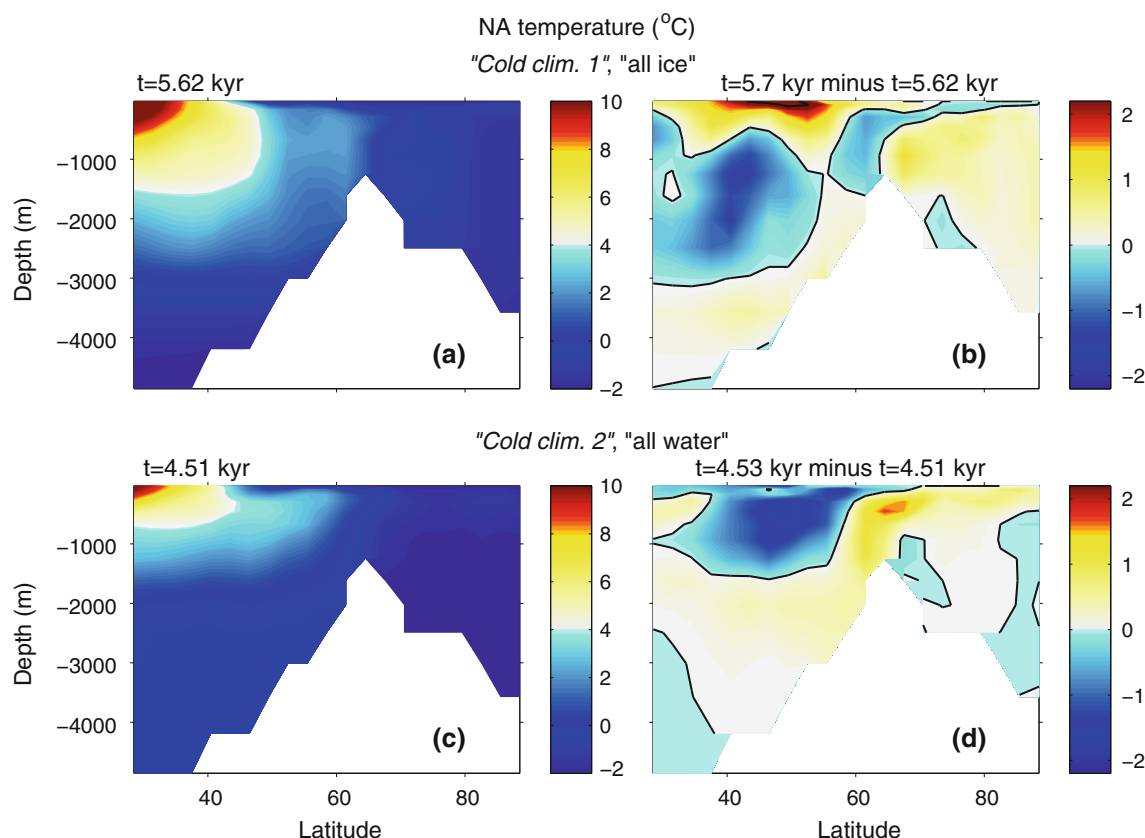


**Fig. 11** The NA water temperature before the MOC transitions (a, c) and difference between the temperature after and before the MOC transitions (b, d), indicated by the vertical dashed lines in

Figs. 7 and 8, for the “cold climate 1” “all ice” (a, b) and “cold climate 2” “all water” (c, d) runs. The black contour line indicates the zero value

compared to the temperature before the transition. The stronger MOC after the transition enhances the advection of warm water from low to high latitudes, affecting the stratification and influencing deep water temperature as well.

An opposite picture is seen between 65 and 80°N. As for the “cold climate 2” “all water” run, the surface water is colder and the deep water (of depth  $\sim 2,000$  m) is warmer after the MOC transition, consistent with the weaker MOC after the transition. The water becomes warmer for latitudes higher than  $\sim 60^\circ\text{N}$ . The picture for salinity is simpler (Fig. 12) where the salinity of the high latitudes of the NA under stronger MOC states is relatively high due to advection from low latitudes.

## 5 Discussion and conclusions

We explored multiple sea-ice states in a state-of-the-art ocean GCM for different basic states, including present-day like and colder climate conditions that were prescribed via the extent of land ice and atmospheric  $\text{CO}_2$ .

The GCM includes sea-ice dynamics and thermodynamics; it is coupled to an atmospheric energy and moisture balance model and has a realistic bathymetry and land configuration. For each cold and warm climate state, we perturbed the initial spun-up state twice by eliminating all sea ice (“all water”) and by prescribing a global initial sea ice cover (“all ice”) and ran these models into steady state. No significant NH multiple sea-ice states were observed in our model under present-day like conditions. However, when repeating the experiments under colder climate conditions, two distinct NH steady-state sea-ice states were found, in which the zonally averaged meridional sea-ice extent differs by a modest amount of about three degrees latitude. For the SH two sea-ice states that differed from each other by three to four degrees in latitudinal extent were observed for all experiments. Previous studies reported multiple states of sea ice such as a global sea ice cover, ice-free ocean and intermediate sea-ice cover. We show here that it is possible to obtain multiple states of sea ice that all correspond to an intermediate sea-ice cover and may be relevant to glacial climate dynamics.

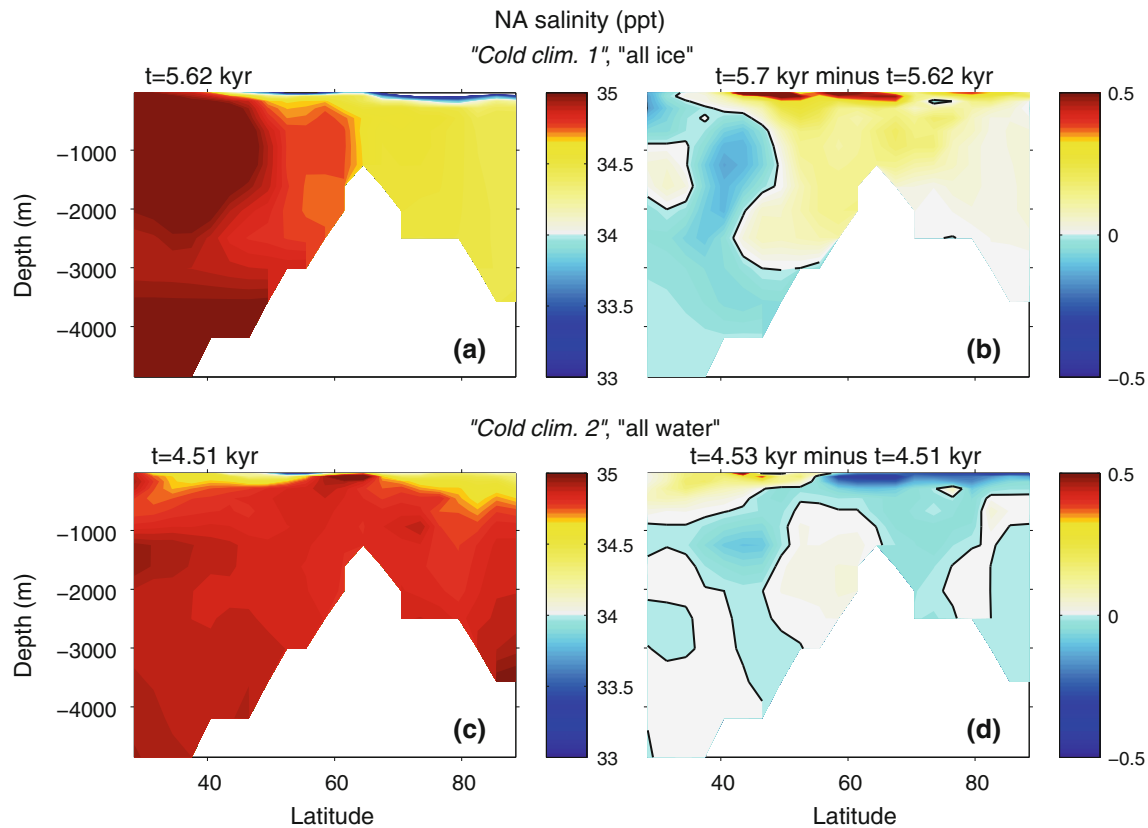


**Fig. 12** The NA water salinity before the MOC transitions (a, c) and difference between the salinity after and before the MOC transitions (b, d), indicated by the vertical dashed lines in Figs. 7 and 9, for the

“cold climate 1” “all ice” (a, b) and “cold climate 2” “all water” (c, d) runs. The black contour line indicates the zero value

While our results support the hypothesis of multiple sea-ice states (both in the NH and SH) under sufficiently cold conditions, the difference between the states, up to four degrees latitude, may be too small to support the sea-ice switch mechanism (Gildor and Tziperman 2000). However, the atmospheric model used here is simple and many feedbacks involving air-sea interaction are missing (e.g., the winds are constant in this model). It is possible, therefore, that with a more realistic atmospheric model, different multiple sea-ice states (more or less pronounced) may be observed. We used annual-averaged forcing, and multiple equilibria that exist under such conditions may disappear once seasonal forcing is introduced, due to the large seasonal cycle in sea ice extent. It is instructive, though, to first perform this study without a seasonal cycle as done here, before proceeding to the more realistic case.

We observed abrupt transitions between a warm state associated with a strong MOC and a small sea-ice cover, and a cold state with a weaker MOC and a larger sea-ice cover. The transitions are between quasi-steady states, although one could envision these states to be even more stable and longer-lasting in a different model configuration with different model parameters. Such transitions were previously suggested to be a

possible mechanism for the climate signal of DO and Heinrich events (Kaspi et al. 2004; Dansgaard et al. 1989; Alley et al. 1993; Bond et al. 1992; Heinrich 1988). In particular, these studies showed that small MOC changes can lead to a finite sea-ice response, which then leads to a dramatic atmospheric temperature response, consistent with the proxy record of DO events (see also Li et al. 2005).

As mentioned in Sect. 4, the interaction between MOC and sea ice was discussed in many previous studies, mainly in relation to DO events. The results reported here are relevant to some of these studies. First, the steady states of the MOC and sea ice are stable after a transient period—we have extended the runs to cover a time period of 10 kyr and did not observe variations in the steady states. Our results are different from some of these previous studies that reported that the cold state is more unstable than the warm state, though the difference may be due to the simple atmospheric model and annual mean forcing used here. Second, as depicted in Fig. 7c, f, the cold state is not always unstable. We find that, before converging to the final states, the MOC switches from a strong to a weak state and the sea-ice cover becomes more extended at this transition.

There are at least two main mechanisms that are candidates for generating multiple sea-ice states. The first is the ice-albedo feedback, and the second is linked to MOC dynamics and multiple-equilibria. In studies that reported very different sea-ice states, for example, Martozke and Botzet (2007) and Ferreira et al. (2011), these different states are mainly associated with the ice-albedo effect because for global scale sea-ice differences the ice-albedo effect is more important. Multiple sea-ice states that do not differ from each other on a global scale (such as those associated with DO events) are more likely linked to MOC dynamics. The NH multiple sea-ice states reported here are at least partially associated with MOC changes. It is interesting to note that multiple sea-ice states are observed here (although with small differences between them) even after the different MOC states have relaxed to almost the same state. In addition, we observed interesting multiple sea-ice states in the southern hemisphere, which warrant further investigation not possible here.

**Acknowledgments** This work was supported by the Israel-US Binational Science foundation. ET was supported by the NSF climate dynamics program, grants ATM-0754332 and ATM-0902844 and thanks the Weizmann institute for its hospitality during parts of this work. We thank Ian Eisenman for helpful discussions and suggestions and André Paul for help with implementing the EMBM.

## References

- Abbot D, Voigt A, Koll D (2011) The Jormungand global climate state and implications for neoproterozoic glaciations. *J Geophys Res* 116:D18,103
- Adcroft A, Campin JM, Hill C, Marshall J (2004) Implementation of an atmosphere-ocean general circulation model on the expanded spherical cube. *Mon Weath Rev* 132(12):2845–2863
- Alley RB, Meese D, Shuman C, Gow AJ, Taylor K, Grootes P, White J, Ram M, Waddington ED, Mayewski P, Zielinski G (1993) Abrupt increase in Greenland snow accumulation at the end of the Younger Dryas event. *Nature* 362:527–529
- Arzel O, Colin de Verdière A, England MH (2010) The role of oceanic heat transport and wind-stress forcing in abrupt millennial-scale climate transitions. *J Clim* 23(9):2233–2256
- Arzel O, England MH, Saenko O (2011) The impact of wind-stress feedback on the stability of the Atlantic meridional overturning circulation. *J Clim* 24:1965–1984
- Ashkenazy Y, Tziperman E (2004) Are the 41 kyr glacial oscillations a linear response to Milankovitch forcing? *Quat Sci Rev* 23(18–19):1879–1890
- Ashkenazy Y, Tziperman E (2007) A wind-induced thermohaline circulation hysteresis and millennial variability regimes. *J Phys Oceanogr* 37(10):2446–2457
- Bond G, Heinrich H, Broecker W, Laberie L, McManus J, Andrews J, Huon S, Jantschik R, Clasen S, Simet C, Tedesco K, Klas M, Bonani G, Ivy S (1992) Evidence for massive discharges of icebergs into the North Atlantic Ocean during the last glacial period. *Nature* 360(6401):245–249
- Bryan K (1984) Accelerating the convergence to equilibrium of ocean-climate models. *J Phys Oceanogr* 14:666–673
- Campin JM, Marshall J, Ferreira D (2008) Sea-ice ocean coupling using a rescaled vertical coordinate  $z^*$ . *Ocean Model* 24(1–2):1–14
- Colin de Verdière A, Te Raa L (2010) Weak oceanic heat transport as a cause of the instability of glacial climates. *Clim Dyn* 35(7–8):1237–1256
- Dansgaard W, White J, Johnsen S (1989) The abrupt termination of the Younger Dryas climate event. *Nature* 339:532–534
- Eisenman I, Wettlaufer J (2009) Nonlinear threshold behavior during the loss of Arctic sea ice. *Proc Natl Acad Sci USA* 106:28–32
- EPICA-Community-Members (2004) Eight glacial cycles from an antarctic ice core. *Nat Biotechnol* 429:623–628
- Fanning AF, Weaver AJ (1996) An atmospheric energy-moisture balance model: climatology and interpentadal climate change, and coupling to an OGCM. *J Geophys Res* 101(D10):15111–15125
- Ferreira D, Marshall J, Rose BEJ (2011) Climate determinism revisited: multiple equilibria in a complex climate model. *J Clim* 24:992–1012
- Gent PR, McWilliams JC (1990) Isopycnal mixing in ocean circulation models. *J Phys Oceanogr* 20(1):150–155
- Ghil M (1994) Cryothermodynamics: the chaotic dynamics of paleoclimate. *Physica D* 77:130–159
- Gildor H (2003) When Earth's freezer door is left ajar. *EOS* 84(23):215
- Gildor H, Tziperman E (2000) Sea ice as the glacial cycles climate switch: role of seasonal and orbital forcing. *Paleoceanography* 15:605–615
- Gildor H, Tziperman E (2001) Physical mechanisms behind biogeochemical glacial-interglacial  $CO_2$  variations. *Geophys Res Lett* 28:2421–2424
- Gildor H, Tziperman E (2003) Sea-ice switches and abrupt climate change. *Philos Trans R Soc London Ser A Math Phys Eng Sci* 361(1810):1935–1942
- Heinrich H (1988) Origin and consequences of cyclic ice rafting in the Northeast Atlantic Ocean during the past 130,000 years. *Quat Res* 29:142–152
- Hibler WD (1980) Modeling a variable thickness sea ice cover. *Mon Weath Rev* 108:1943–1973
- Holland MM, Bitz CM, Hunke EC, Lipscomb WH, Schramm JL (2006a) Influence of the sea ice thickness distribution on polar climate in CCSM3. *J Clim* 19(11):2398–2414
- Holland MM, CM Bitz, Tremblay B (2006b) Future abrupt reductions in the summer Arctic sea ice. *Geophys Res Lett* 33:L23,503
- Imbrie J, Hays J, Martinson D, McIntyre A, Mix A, Morley J, Pisias N, Prell W, Shackleton N (1984) The orbital theory of pleistocene climate: support from a revised chronology of the marine  $\delta^{18}O$  record. In: Berger A, Imbrie J, Hays J, Kukla G, Saltzman B (eds) *Milankovitch and climate, Part I*, D. Reidel, Dordrecht, pp 269–305
- Kaspi Y, Sayag R, Tziperman E (2004) A “triple sea-ice state” mechanism for the abrupt warming and synchronous ice sheet collapses during Heinrich events. *Paleoceanography* 19(3):PA3004. doi:10.1029/2004PA001009
- Langen PL, Alexeev VA (2004) Multiple equilibria and asymmetric climates in the ccm3 coupled to an oceanic mixed layer with thermodynamic sea ice. *Geophys Res Lett* 31:L04201
- Large WG, McWilliams JC, Doney SC (1994) Oceanic vertical mixing: a review and a model with a nonlocal boundary-layer parameterization. *Rev Geophys* 32(4):363–403
- Lenton TM, Held H, Kriegler E, Hall JW, Lucht W, Rahmstorf S, Schellnhuber HJ (2008) Tipping elements in the Earth's climate system. *Proc Natl Acad Sci USA* 105:1786–1793
- Levitus SE (1982) *Climatological atlas of the world ocean*. NOAA Professional Paper 13 US Government Printing Office, Washington, DC

- Li C, Battisti D, Schrag D, Tziperman E (2005) Abrupt climate shifts in Greenland due to displacements of the sea ice edge. *Geophys Res Lett* 32:L19702
- Lindsay RW, Zhang J (2005) The thinning of arctic sea ice, 1988–2003: have we passed a tipping point?. *J Clim* 18:4879–4894
- Losch M, Menemenlis D, Heimbach P, Campin JM, Hill C (2010) On the formulation of sea-ice models. part 1: effects of different solver implementations and parameterizations. *Ocean Model* 33:129–144
- Loving JL, Vallis GK (2005) Mechanisms for climate variability during glacial and interglacial periods. *Paleoceanography* 20(4):PA4024
- Manabe S, Stouffer RJ (1999) The role of the thermohaline circulation in climate. *Tellus* 51:91–109
- Marotzke J, Botzet M (2007) Present-day and ice-covered equilibrium states in a comprehensive climate model. *Geophys Res Lett* 34:L16704
- Marshall J, Adcroft A, Hill C, Perelman L, Heisey C (1997a) A finite-volume, incompressible Navier stokes model for studies of the ocean on parallel computers. *J Geophys Res* 102, C3:5753–5766
- Marshall J, Hill C, Perelman L, Adcroft A (1997b) Hydrostatic, quasi-hydrostatic, and nonhydrostatic ocean modeling. *J Geophys Res* 102(C3):5733–5752
- Maslanik JA, Fowler C, Stroeve J, Drobot S, Zwally J, Yi D, Emery W (2007) A younger, thinner Arctic ice cover: Increased potential for rapid, extensive sea-ice loss. *Geophys Res Lett* 34:L24501
- Merryfield WJ, Holland MM, Monahan AH (2008) Multiple equilibria and abrupt transitions in Arctic summer sea ice extent. In: DeWeaver E, Bitz CM, Tremblay B (eds) *Arctic sea ice decline: observations, projections, mechanisms, and implications*. Geophysical Monograph Series, vol 180. AGU, Washington, D.C., pp 151–174
- MITgcm Group (2010) MITgcm user manual. Online documentation, MIT/EAPS, Cambridge, MA 02139, USA, [http://mitgcm.org/public/r2\\_manual/latest/online\\_documents/manual.html](http://mitgcm.org/public/r2_manual/latest/online_documents/manual.html)
- Mix AC, Bard E, Schneider R (2001) Environmental processes of the ice age: land, oceans, glaciers (EPILOG). *Quat Sci Rev* 20:627–657
- Overpeck JT, Strum M, Francis JA, Perovich DK, Serreze MC, Benner R, Carmack EC, Chapin FS, Gerlach SC, Hamilton LC, Hinzman LD, Holland M, Huntington HP, Key JR, Lloyd AH, McDonald GM, McFadden J, Noone D, Prowse TD, Schlosser P, Vörösmarty C (2005) Arctic system on trajectory to new, seasonally ice-free state. *EOS Trans Am Geophys Union* 86(34):309–313
- Peltier WR (1994) Ice age paleotopography. *Science* 265:195–201
- Petit JR, Jouzel J, Raynaud D, Barkov NI, Barnola JM, Basile I, Bender M, Chappellaz J, Davis M, Delaygue G, Delmotte M, Kotlyakov VM, Legrand M, Lipenkov VY, Lorius C, Pepin L, Ritz C, Saltzman E, Stievenard M (1999) Climate and atmospheric history of the past 420,000 years from the Vostok ice core, Antarctica. *Nature* 399:429–436
- Ram M, Koenig G (1997) Continuous dust concentration profile of pre Holocene ice from the Greenland ice sheet project 2 ice core: dust stadials, interstadials, and the Eemian. *J Geophys Res* 102:26641–26648
- Redi MH (1982) Oceanic isopycnal mixing by coordinate rotation. *J Phys Oceanogr* 12:1154–1158
- Sayag R, Tziperman E, Ghil M (2004) Rapid switch-like sea ice growth and land ice–sea ice hysteresis. *Paleoceanography* 19:PA1021. doi:[10.1029/2003PA000946](https://doi.org/10.1029/2003PA000946)
- Schmittner A, Meissner KJ, Eby M, Weaver AJ (2003) Forcing of the deep ocean circulation in simulations of the last glacial maximum. *Paleoceanography* 17(2):1015
- Semtner AJ (1976) A model for the thermodynamic growth of sea ice in numerical investigations of climate. *J Phys Oceanogr* 6
- Serreze MC, Francis JA (2006) The Arctic amplification debate. *Clim Change* 76:241–264
- Tietsche S, Notz D, Jungclaus JH, Marotzke J (2011) Recovery mechanisms of Arctic summer sea ice. *Geophys Res Lett* 38:L02707
- Timmermann A, Gildor H, Schulz M, Tziperman E (2003) Coherent resonant millennial-scale climate oscillations triggered by glacial meltwater pulses. *J Clim* 16:2569–2585
- Tziperman E, Gildor H (2003) The mid-Pleistocene climate transition and the source of asymmetry between glaciation and deglaciation times. *Paleoceanography* 18(1). doi:[10.1029/2001PA000627](https://doi.org/10.1029/2001PA000627)
- Tziperman E, Raymo M, Huybers P, Wunsch C (2006) Consequences of pacing the Pleistocene 100 kyr ice ages by nonlinear phase locking to Milankovitch forcing. *Paleoceanography* 21:PA4206. doi:[10.1029/2005PA001241](https://doi.org/10.1029/2005PA001241)
- Wang Z, Mysak L (2006) Glacial abrupt climate changes and Dansgaard–Oeschger oscillations in a coupled climate model. *Paleoceanography* 21(2):PA2001
- Weaver AJ, Eby M, Wiebe EC, Bitz CM, Duffy PB, Ewen TL, A F Fanning MMH, MacFadyen A, HD Matthews KM, Saenko O, Schmittner A, Wang H, Yoshimori M (2001) The UVic earth system climate model: model description, climatology and application to past, present and future climates. *Atmos Ocean* 39:361–428
- Winton M (1993) Deep decoupling oscillations of the oceanic thermohaline circulation. In: Peltier WR (ed), *Ice in the climate system*, NATO ASI series I: global environmental, change, vol 12, Springer, Berlin, pp 417–432
- Winton M, Sarachik ES (1993) Thermohaline oscillation induced by strong steady salinity forcing of ocean general circulation models. *J Phys Oceanogr* 23:1389–1410
- Wunsch C (2003) The spectral description of climate change including the 100 ky energy. *Clim Dyn* 20:353–363. doi:[10.1007/s00382-002-0279-z](https://doi.org/10.1007/s00382-002-0279-z)